arXiv:1405.6784v1 [nucl-th] 27 May 2014

Microscopic description of fission in neutron-rich plutonium isotopes with the Gogny-D1M energy density functional

R. Rodríguez-Guzmán*
Department of Physics and Astronomy, Rice University, Houston, Texas 77005, USA and
Department of Chemistry, Rice University, Houston, Texas 77005, USA

L.M. Robledo
Departamento de Física Teórica, Universidad Autónoma de Madrid, 28049-Madrid, Spain†
(Dated: May 28, 2014)

The most recent parametrization D1M of the Gogny energy density functional is used to describe fission in the isotopes $^{232-280}$Pu. We resort to the methodology introduced in our previous studies [Phys. Rev. C **88**, 054325 (2013) and Phys. Rev. C **89**, 054310 (2014)] to compute the fission paths, collective masses and zero point quantum corrections within the Hartree-Fock-Bogoliubov framework. The systematics of the spontaneous fission half-lives t_{SF}, masses and charges of the fragments in Plutonium isotopes is analyzed and compared with available experimental data. We also pay attention to isomeric states, the deformation properties of the fragments as well as to the competition between the spontaneous fission and α-decay modes. The impact of pairing correlations on the predicted t_{SF} values is demonstrated with the help of calculations for $^{232-280}$Pu in which the pairing strengths of the Gogny-D1M energy density functional are modified by 5 % and 10 %, respectively. We further validate the use of the D1M parametrization through the discussion of the half-lives in $^{242-262}$Fm. Our calculations corroborate that, though the uncertainties in the absolute values of physical observables are large, the Gogny-D1M Hartree-Fock-Bogoliubov framework still reproduces the trends with mass and/or neutron numbers and therefore represents a reasonable starting point to describe fission in heavy nuclear systems from a microscopic point of view.

PACS numbers: 24.75.+i, 25.85.Ca, 21.60.Jz, 27.90.+b

I. INTRODUCTION

Nuclear fission is a large amplitude collective phenomenon whose full understanding still remains as one of the main challenges in nuclear structure physics. On the way to scission into two or more fragments, the nuclear shapes evolve through a multidimensional landscape that can be described in terms of several deformation parameters [1–4]. Within this context, our present knowledge of nuclear fission owes a lot to the efforts to incorporate the stabilizing role of shells effects into the semiclasical liquid drop model (see, for example, Refs. [5, 6] and references therein). The potential energy surfaces provided by such models emphasize the key role played by several kinds of nuclear configurations, intimately related to shells effects, along the fission path to determine observables like the spontaneous fission half-life and the mass distribution of the fragments [5]. Such configurations comprise minima, valleys, ridges and saddle points. For example, local minima can affect the dynamics and time scale of the fission process. In particular, both (superdeformed) first and (hyperdeformed) second isomeric states have been the subject of intense debate [7–18].

Though quite sophisticated approximations have already been invoked [19, 20], the constrained self-consistent mean-field approximation [21, 22] has emerged as a poweful framework for systematic microscopic studies of real fissioning nuclei in terms of non-relativistic Gogny [15, 18, 23–29], Skyrme [16, 30–33] and BCPM-like [17] as well as relativistic [34–37] Energy Density Functionals (EDFs). Here, the multidimensional fission landscape is determined in terms of constraints on multipole moments and neck parameters. The approximation also provides the required ingredients to obtain the collective inertias as well as the zero point energy quantum corrections [18] stemming from the restoration of the symmetries broken in the corresponding mean-field states through the spontaneous symmetry breaking mechanism [21]. It also accounts for quantum mechanical tunneling effects. Such microscopic studies assume that fission properties are determined by general features of the considered EDFs and are quite demaning from the computational point of view, a task that has been greatly helped by recent developments in the field of high-performance computing.

From the theoretical point of view, a better description of the fission process is required to account for shell effects and/or magic numbers in heavy and superheavy nuclear systems [33, 38]. On the other hand, microscopic studies of the spontaneous fission and α-decay modes [29, 31] are important to better understand the stability of heavy and superheavy elements. The last ones have been the subject of intense experimental effort in recent years (see, for example, Refs. [39–41] and references therein). Beside the unique insight that such superheavy

*Electronic address: raynerrobertorodriguez@gmail.com
†Electronic address: luis.robledo@uam.es

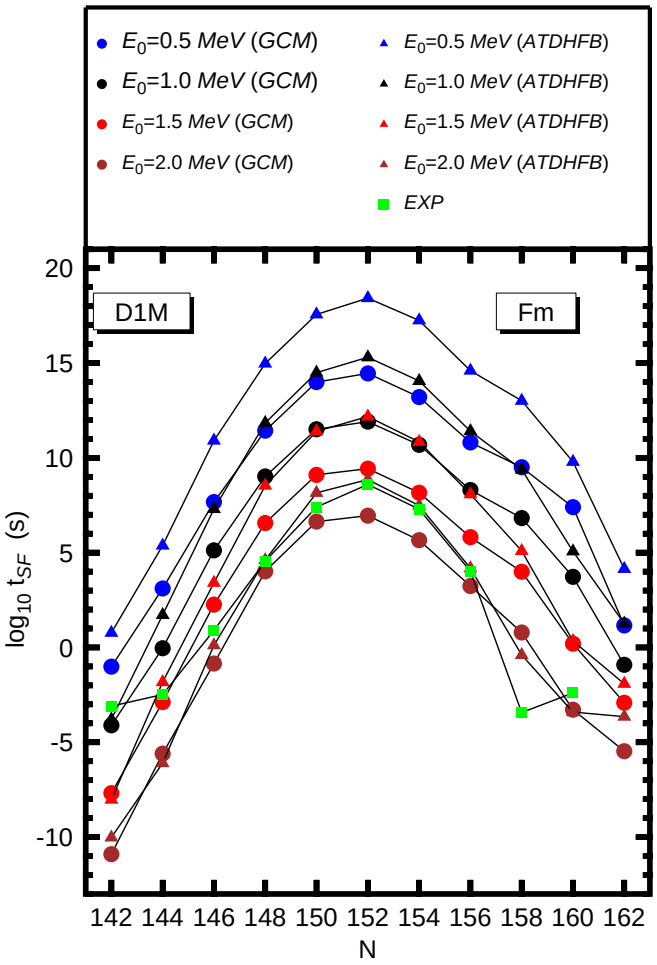

FIG. 1: (Color online) The spontaneous fission half-lives t_{SF}, predicted within the GCM and ATDHFB schemes, for the isotopes $^{242-262}$Fm are depicted as functions of the neutron number. Results have been obtained with the Gogny-D1M EDF. Calculations have been carried out with E_0=0.5, 1.0, 1.5 and 2.0 MeV, respectively. The available experimental t_{SF} values [44] are included in the plot. For more details, see the main text.

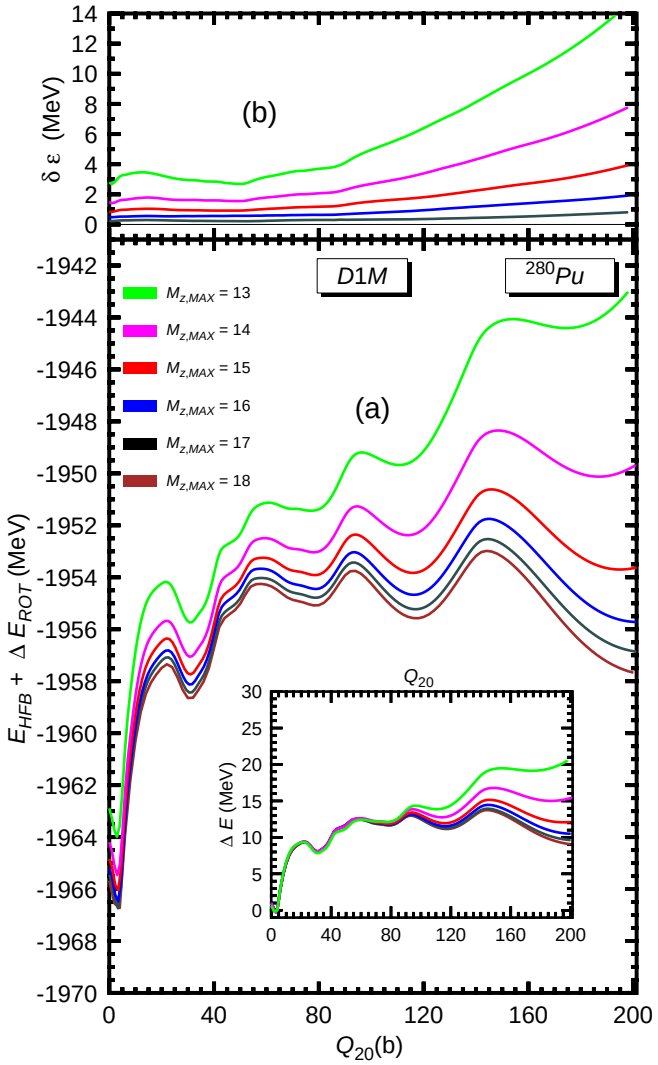

FIG. 2: (Color online) The rotationally corrected energies $E_{HFB} + \Delta E_{ROT}$ corresponding to the 1F configurations in ^{280}Pu are shown in panel (a) as functions of the quadrupole moment Q_{20}. Results are shown for $M_{z,MAX}$=13, 14, 15, 16, 17 and 18, respectively. The inset in panel (a) displays, for each $M_{z,MAX}$, the relative energies referred to the corresponding ground states. The energy differences with respect to the calculations with $M_{z,MAX}$=18 are depicted in panel (b). For more details, see the main text.

elements provide on nuclear structure properties under extreme conditions [33], one shoud also keep in mind that they are produced during the r-process and their properties determine the upper end of the nucleosynthesis flow [42]. The wealth of information in actinide nuclei [1] as well as progress in several areas of science and applications [3, 4] also act as driving forces to improve our models for nuclear fission. In addition, microscopic fission studies of neutron-rich nuclei are also required since, on the one hand, these are the territories where the fate of the nucleosynthesis of heavy nuclei is determined and, on the other hand, such systems represent a challenging testing ground to examine the adequacy of nuclear effective interactions when extrapolated to exotic N/Z ratios.

In our previous work [18], we have performed dripline-to-dripline fission calculations for Uranium isotopes as well as for a selected set of heavy and superheavy nuclei for which experimental data are available [7, 43–46] . We have carried out a detailed comparison between the results obtained with the most standard parametrization of the Gogny-EDF [47] (i.e., D1S [23]) and the ones provided by the new parametrizations D1N [48] and D1M [49], respectively. The comparison between Gogny-like EDFs, with available data for barrier heights, excitation energies of fission isomers and half-lives as well as with previous theoretical studies [15, 17, 28, 29] have shown that the Gogny-D1M EDF represents a reasonable starting point to describe fission in heavy and superheavy nu-

clei. This is quite satisfying as the parametrization D1M does a much better job to reproduce nuclear masses [49] and, at the same time, seems to reproduce low energy nuclear structure data with the same or better accuracy than the well tested D1S parametrization [49–56]. We have also paid special attention to the uncertainties in the determination of the absolute values of fission observables [17, 18]. Such uncertainties are presumed to be large. However, it has been shown that the mean-field approximation reproduces reasonably well the trend of fission observables as functions of the mass number and/or along isotoptic chains.

In the present work we have used the Hartree-Fock-Bogoliubov (HFB) approximation [21], based on the Gogny-D1M EDF [49], to carry out fission calculations along the Plutonium isotopic chain, including very neutron-rich isotopes. To this end, we have considered the nuclei $^{232-280}$Pu. We have used the same methodology as in Ref. [18]. Therefore, all the calculations to be discussed later on are subject to the same uncertainties already described in that reference. However this study is, to the best of our knowlegde, the first one in which the Gogny-D1M EDF is systematically employed to describe fission in neutron-rich Plutonium isotopes. Second, it will allow us to see to which extent the physical trends already obtained for Uranium isotopes [18], using this particular version of the Gogny-EDF, hold for other nuclei in the same region of the nuclear chart. Third, we discuss the appearence of second fission isomers in the corresponding one-fragment curves of Plutonium nuclei. Having in mind that fission observables are quite sensitive to pairing correlations [17, 18], due to the strong dependence of the collective inertias with the inverse of the pairing gap [57, 58] , we have also carried out self-consistent HFB calculations for the nuclei $^{232-280}$Pu using a modified Gogny-D1M EDF in which the strenghts of the neutron and proton pairing fields are increased by 5 % and 10 %, respectively. We also pay attention to the competition between the spontaneous fission and α-decay channels along the Plutonium chain. Last, but not least, we further validate the use of the Gogny-D1M EDF in fission studies, by comparing the spontaneous fission half-lives predicted for the nuclei $^{242-262}$Fm with the available experimental data [44]. For the convenience of the reader, and also to facilitate the comparison with Uranium isotopes, we keep the style of our discussions as close as possible to the one used in Ref. [18].

The paper is organized as follows. In Sec. II, we briefly outline the theoretical framework used in the present study. For more details the interested reader is referred to Ref. [18]. In this section, we will also compare Gogny-D1M spontaneous fission half-lives for the nuclei $^{242-262}$Fm with the available experimental values. The results of our calculations for the isotopes $^{232-280}$Pu are discussed in Sec. III. First, in Sec. III A, we discuss the convergence of the calculations in terms of the basis size in the case of the very neutron-rich nucleus ^{280}Pu. We start section III B, with a detailed description of our

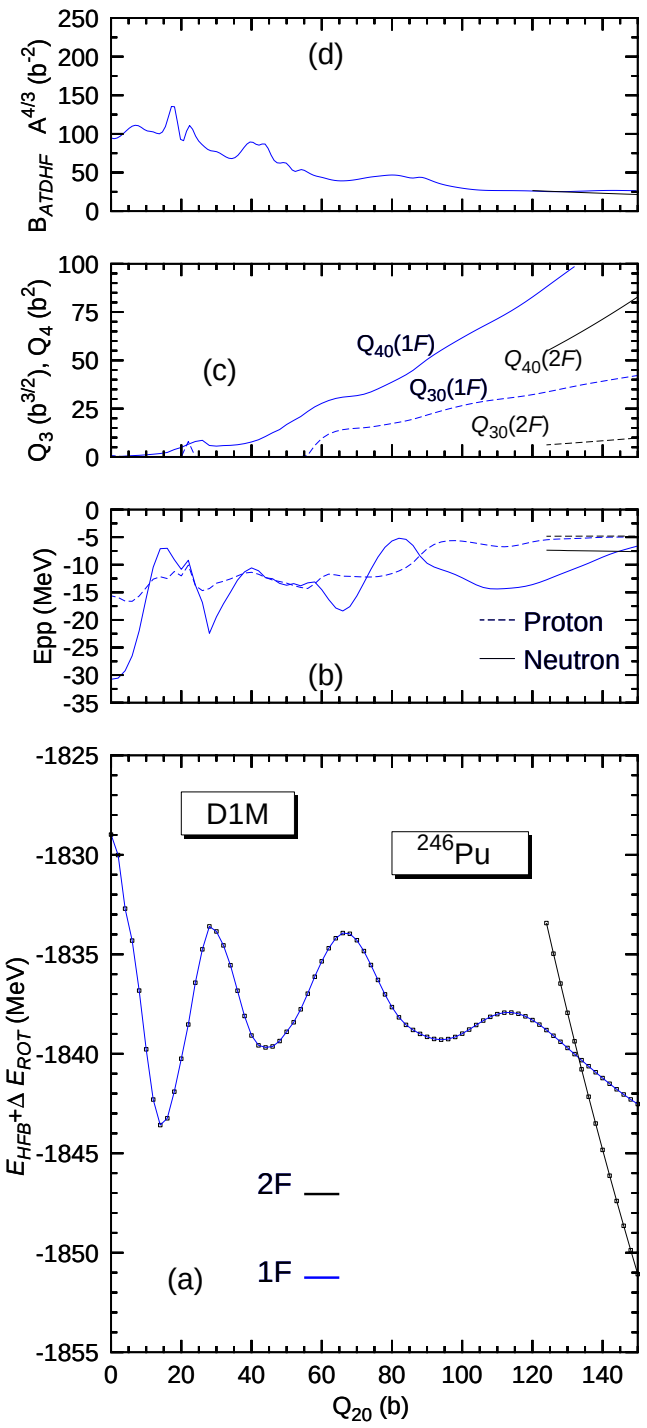

FIG. 3: (Color online) The HFB plus the zero point rotational energies obtained with the Gogny-D1M EDF are plotted in panel (a) as functions of the quadrupole moment Q_{20} for the nucleus ^{246}Pu. Both the one (1F) and two-fragment (2F) solutions are included in the plot. The pairing interaction energies are depicted in panel (b) for protons (dashed lines) and neutrons (full lines). The octupole and hexadecapole moments corresponding to the 1F and 2F solutions are given in panel (c). The collective masses obtained within the ATDHFB approximation are plotted in panel (d). For more details, see the main text.

fission calculations for the nucleus ^{246}Pu taken as an illustrative example. Next, we present the systematics of the fission paths, spontaneous fission half-lives and fragment's charge and mass for the considered Plutonium isotopes. In the same section we will also discuss the appearence of second isomeric states in Plutonium nuclei. In Sec. III C, we explicitly discuss the impact of pairing correlations on the predicted spontaneous fission half-lives for $^{232-280}$Pu by increasing artificially the pairing strengths of the original Gogny-D1M EDF. Conclusions and work perspectives are presented in Sec. IV.

II. THEORETICAL FRAMEWORK

As already mentioned, we have resorted to the constrained HFB approximation [21]. We have used as constraining operators the axially symmetric quadrupole $\hat{Q}_{20} = z^2 - \frac{1}{2}\left(x^2+y^2\right)$ and octupole $\hat{Q}_{30} = z^3 - \frac{3}{2}\left(x^2+y^2\right)z$ [50, 51] operators to obtain the corresponding one-fragment (1F) solutions. On the other hand, constraints on the necking $\hat{Q}_{Neck}(z_0, C_0) = \exp\Big[-\left(z-z_0\right)^2/C_0^2\Big]$ operator are used to reach two-fragment (2F) solutions [17, 18, 28]. We have also considered a constraint on the operator $\hat{Q}_{10} = rP_1\left(cos(\theta)\right)$, to avoid spurious effects associated to the center of mass motion [50, 51]. Finally the typical HFB constraints on both the proton and neutron numbers [21] are considered.

The quasiparticle operators [21] have been expanded in a deformed axially symmetric harmonic oscillator (HO) basis containing states with J_z quantum numbers up to 35/2 and up to 26 quanta in the z direction. The basis quantum numbers are restricted by the condition

$$2n_\perp + |m| + \frac{1}{q}n_z \leq M_{z,Max} \tag{1}$$

with $M_{z,Max}$=17 and q=1.5. For each of the fission configurations in $^{232-280}$Pu and $^{242-262}$Fm, the HO lengths b_z and $b_\perp$ have been optimized so as to minimize the total HFB energies. Both the choice of the basis size and the minimization of the energy with respect to the oscillator lengths b_z and $b_\perp$ lead to well converged relative energies (see below). For the solution of the HFB equations, an approximate second order gradient method [50–52, 59] has been used. The Coulomb exchange term has been considered in the Slater approximation [60, 61] while the spin-orbit contribution to the pairing field has been neglected.

In order to obtain the corresponding fission paths for the considered Plutonium and Fermium nuclei, we have employed the methodology outlined in our previous studies [17, 18], i.e.,

- we have first carried out reflection-symmetric Q_{20}-constrained calculations. Subsequently, for each quadrupole deformation Q_{20}, we have constrained to a large Q_{30} value and then released such a constraint to reach the lowest energy solution. In this way, we have obtained the 1F solutions.
- for sufficiently large quadrupole moments, we have constrained the number of particles in the neck of the parent nucleus to a small value and then released the constraint self-consistently. Calculations have been carried out with different neck parameters z_0 and C_0 to ensure that the same lowest energy solution is always reached. In this way, we have obtained the 2F configurations for which the charge and mass of the fragments lead to the minimum energy.

Though explicit contraints are not included for them, the average values of higher multipolarity moments (i.e., $\hat{Q}_{40}, \hat{Q}_{60}, \dots$) are automatically adjusted during the self-consistent minimization of the HFB energy. Note, that kinks and multiple branches are common in this type of calculations [18, 62] as a result of projecting multi-dimensional fission paths into a one-dimensional plot. Second, for the same reason, the 1F and 2F curves appear as intersecting ones. However, in the multidimensional space of deformation parameters $\left(\hat{Q}_{20}, \hat{Q}_{30}, \hat{Q}_{Neck}, \dots\right)$, there is a path with a ridge connecting them [23]. We have neglected the small contribution of such a path to the action [see, Eq.(3) below] which amounts to take the 2F curves as really intersecting the 1F ones [17, 18].

The constrained HFB calculations provide all the ingredients required to obtain the collective masses and the zero point energy quantum corrections. To compute the collective mass $B(Q_{20})$ and the zero point vibrational correction $\Delta E_{vib}(Q_{20})$ the perturbative cranking approximation to both the Adiabatic Time Dependent HFB (ATDHFB) approach [63–65] and the Gaussian Overlap Approximation (GOA) to the GCM [21] have been used. The rotational correction $\Delta E_{ROT}(Q_{20})$ has been expressed in terms of the Yoccoz moment of inertia [66–68]. For details, the reader is referred to our previous work [18].

Within the standard Wentzel-Kramers-Brillouin (WKB) formalism [69, 70], the spontaneous fission half-life (in seconds) is given by

$$t_{SF} = 2.86 \times 10^{-21} \times \left(1 + e^{2S}\right) \tag{2}$$

where the action S along the quadrupole constrained fission path reads

$$S = \int_a^b dQ_{20} \sqrt{2B(Q_{20})\left(V(Q_{20}) - (E_{GS} + E_0)\right)} \tag{3}$$

The integration limits a and b correspond to the classical turning points for the energy $E_{GS}+E_0$. The collective potential $V(Q_{20})$ is given by the HFB energy corrected by the zero point rotational $\Delta E_{ROT}(Q_{20})$ and vibrational $\Delta E_{vib}(Q_{20})$ energies.

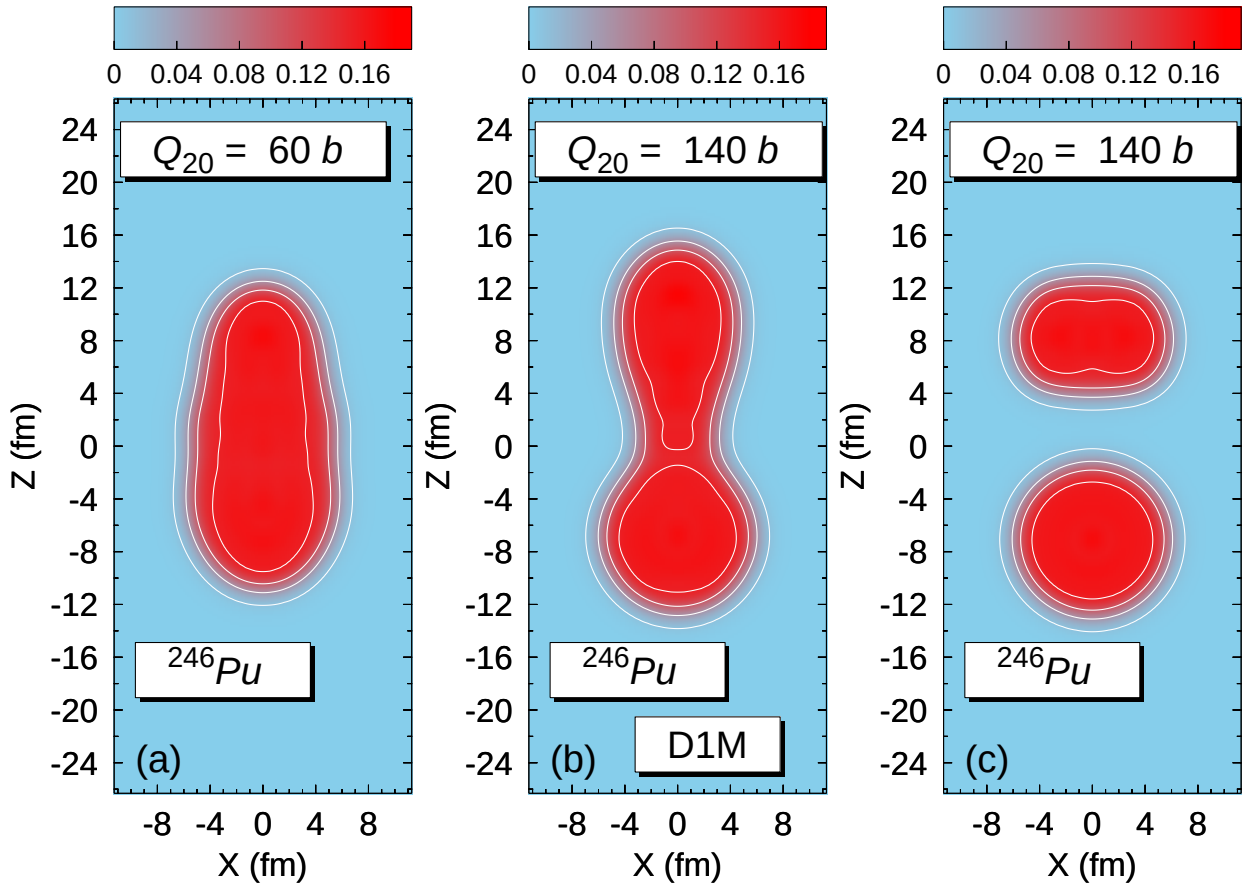

FIG. 4: (Color online) Density contour plots for the isotope ^{246}Pu at the quadrupole deformations Q_{20}=60 b [panel (a)] and Q_{20}=140 b [panels (b) and (c)]. The density contours in panels (a) and (b) correspond to 1F solutions of the HFB equations while the one in panel (c) corresponds to a 2F solution. Results have been obtained with the parametrization D1M of the Gogny-EDF. Densities are in units of fm^{-3} and contour lines are drawn at 0.01, 0.05, 0.10 and 0.15 fm^{-3}.

For the parameter E_0, we have considered four different values, i.e., E_0=0.5, 1.0, 1.5 and 2.0 MeV [18]. In order to analyze the impact of pairing correlations, on both the zero point quantum fluctuations and the collective masses [57, 58], we have also performed self-consistent calculations for the isotopes $^{232-280}$Pu with a modified Gogny-D1M EDF in which the pairing strengths have been increased by 5 % and 10 %, by means of the same multiplicative factor (η=1.05 and 1.10, respectively) in front of the proton and neutron pairing fields [21]. As decay modes spontaneous fission and α-decay compete and determine the stability of heavy nuclear systems [29, 31, 33]. We have computed the α-decay half-lives t_α using the parametrization of the Seaborg-Viola formula given in Ref. [71]. The choice of D1M over D1S is specially justified here as a good description of Q_α values is essential for the Seaborg-Viola formula to perform well.

As already mentioned in the present study we have resorted to the parametrization D1M of the Gogny-EDF whose fitting protocol [49] included both realistic neutron matter equation of state (EoS) information and the binding energies of all known nuclei. In this way, the Gogny-D1M EDF cures a known deficiency of the more standard D1S parametrization [23], i.e., a systematic drift in the differences between experimental and theoretical binding energies in heavy nuclei [72]. This is quite relevant if one keeps in mind that we will extrapolate to very neutron-rich Plutonium isotopes. This is the main reason underlying our choice of the Gogny-D1M EDF in the present study.

To further validate the use of the Gogny-D1M EDF, we have extended our previous t_{SF} calculations (within the GCM and ATDHFB schemes) for Fermium nuclei [18] to the whole set of isotopes $^{242-262}$Fm for which experimental data are available [44]. This chain of isotopes has been studied in previous works. It is considered a very challenging testing ground with competing fission paths (see, for example, Refs. [28, 28, 73] and references therein). We have determined the 1F and 2F curves as well as all the required quantities along the lines described in this section. As can be seen from Fig.1, the predicted t_{SF} values nicely follow the bell-shaped experimental curve. These results corroborate our previous findings [18], i.e., though uncertainties in the corresponding absolute values are large, the Gogny-D1M HFB framework captures

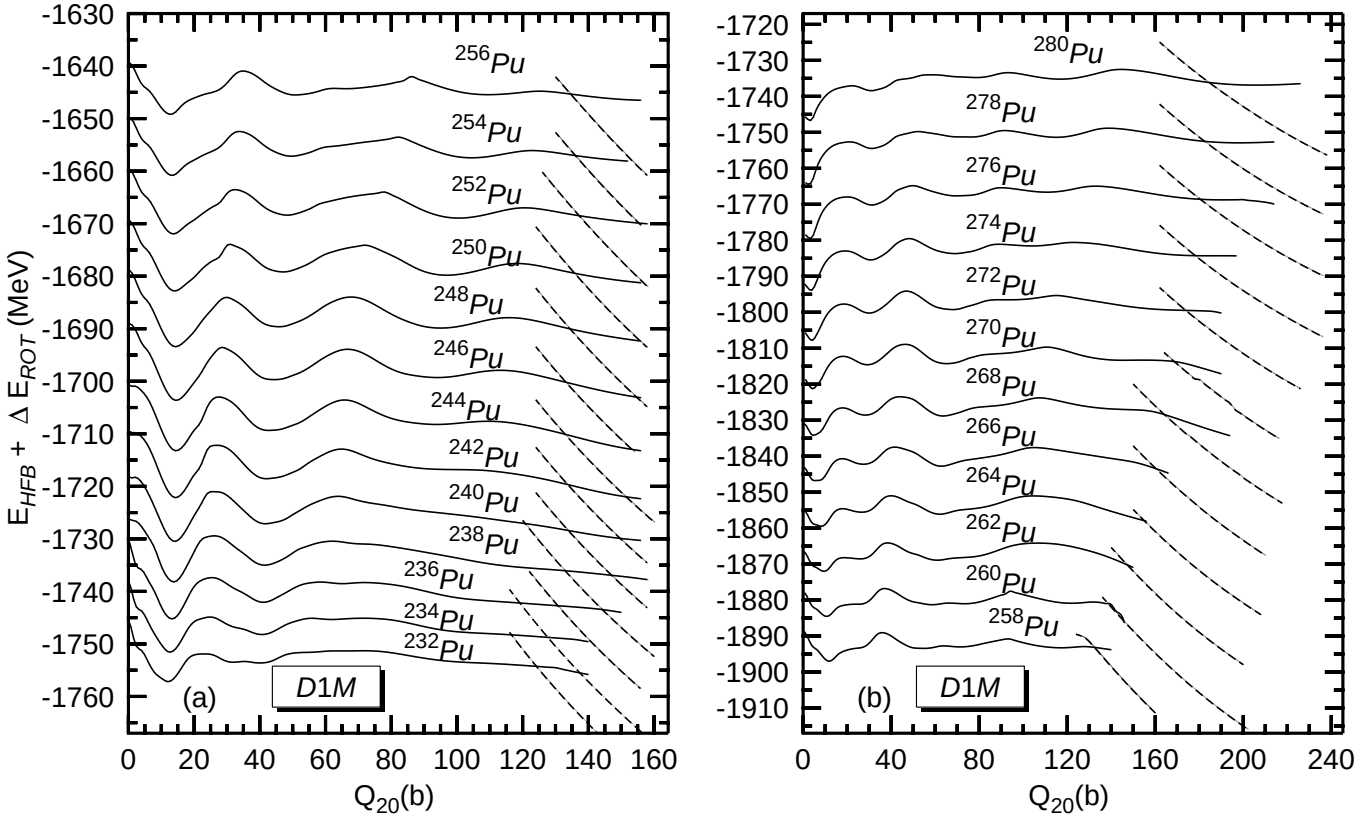

FIG. 5: The HFB plus the zero point rotational energies obtained with the Gogny-D1M EDF are plotted in panel (a) for the nuclei $^{232-256}$Pu and in panel (b) for the nuclei $^{258-280}$Pu as functions of the quadrupole moment Q_{20}. Both the one (1F) and two-fragment (2F) solutions are shown in the plot with continuous and dashed lines, respectively. Starting from ^{234}Pu (^{260}Pu) in panel (a) [in panel (b)] all the curves have been successively shifted by 20 MeV in order to accomodate them in a single plot. Note, the different energy scales in both panels. For more details, see the main text.

the behavior of fission observables like the spontaneous fission half-lives along isotopic chains and represents a reasonable starting point to describe fission in heavy and superheavy nuclei. With this in mind, we have carried out fission calculations for the isotopes $^{232-280}$Pu.

III. DISCUSSION OF THE RESULTS

In this section, we present the results of our Gogny-D1M calculations. In Sec. III A, we discuss the convergence in terms of the basis size in the case of the very neutron-rich isotope ^{280}Pu. First, in Sec. III B, we discuss in detail our results for the nucleus ^{246}Pu, taken as an illustrative example. Subsequenly, we present the systematics of our fission calculations for $^{232-280}$Pu. Finally, in Sec. III C, we will discuss the impact of pairing correlations on the predicted t_{SF} values using a modified Gogny-D1M EDF.

A. Convergence of the calculations

In our calculations, bases with $M_{z,MAX}$=13, 14, 15, 16, 17 and 18 have been used to check the convergence of the results. In all cases we have considered the value q=1.5 and optimized the HO lengths b_z and $b_\perp$. In Fig. 2 (a) we have plotted the rotationally corrected energies E_{HFB} + Δ E_{ROT} corresponding to the 1F configurations in ^{280}Pu as functions of the quadrupole moment Q_{20}. The vibrational energy corrections Δ E_{vib} have not been included in the plot since they are rather constant as functions of the quadrupole moment. The inset in panel (a) displays, for each $M_{z,MAX}$, the relative energies referred to the corresponding ground states. On the other hand, Fig. 2 (b) depicts the energy differences with respect to the calculations with $M_{z,MAX}$=18.

From Fig.2 (a) one concludes that the bases with $M_{z,MAX}$=13, 14 and 15 are too small to describe the 1F configurations in this very neutron-rich isotope at very large quadrupole deformations. On the other hand, larger bases with $M_{z,MAX}$=16, 17 and 18 already provide quite similar profiles for the 1F curves. This is further corroborated from the relative energies shown in the inset. Note, that such relative energies are the ones deter-

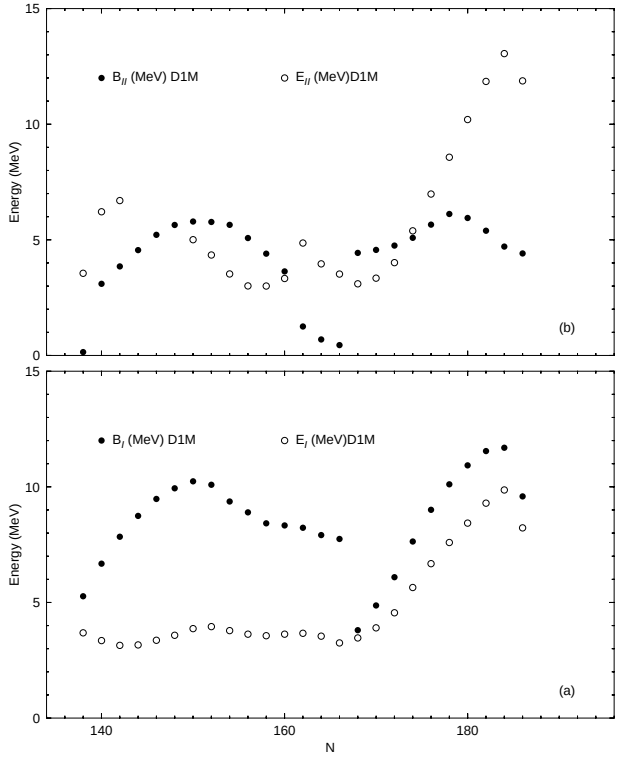

FIG. 6: The excitation energies E_I (E_{II}) and the barrier heights B_I (B_{II}) for the first (second) isomeric wells in $^{232-280}$Pu are plotted in panel (a) [panel (b)] as functions of the neutron number N.

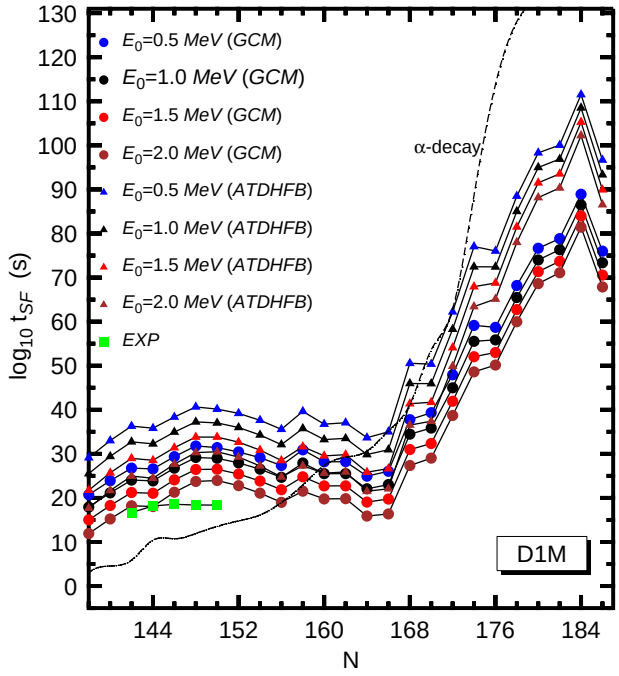

FIG. 7: (Color online) The spontaneous fission half-lives t_{SF}, predicted within the GCM and ATDHFB schemes, for the isotopes $^{232-280}$Pu are depicted as functions of the neutron number. Results have been obtained with the Gogny-D1M EDF. Calculations have been carried out with E_0=0.5, 1.0, 1.5 and 2.0 MeV, respectively. The experimental t_{SF} values [44] for $^{236-244}$Pu are included in the plot. In addition, α-decay half-lives are plotted with short dashed lines. For more details, see the main text.

mining the dynamics of the fission process instead of their absolute values. In fact, a small basis with $M_{z,MAX}$=13 is enough to accurately describe 1F configurations up to $Q_{20} \approx 80$ b while for larger Q_{20} values convergence is only achieved by increasing the basis size. The energy differences $\delta\epsilon$ in Fig.2 (b), show that even for very large Q_{20} values around 200 b, the basis with $M_{z,MAX}$=17 provides an error (with respect to $M_{z,MAX}$=18) always smaller than 0.81 MeV. Similar or even more accurate results also hold for lighter Plutonium isotopes. We have therefore used a basis with $M_{z,MAX}$=17 [18] in all the calculations discussed in the following sections as it provides a reasonable compromise between accuracy and the computational effort required to describe the fission paths in $^{232-280}$Pu.

B. Systematics of fission paths, spontaneous fission half-lives and fragment mass in Plutonium isotopes

In this section, we discuss the systematics of our calculations for the isotopes $^{232-280}$Pu. Let us first describe in more detail the results obtained for the nucleus ^{246}Pu, taken as an illustrative example. In Fig. 3 (a), we show the energies $E_{HFB} + \Delta E_{ROT}$, as functions of Q_{20}, for the 1F and 2F solutions, respectively. The ground state is located at Q_{20}=14 b while a first fission isomer appears at Q_{20}=44 b with an excitation energy of 3.90 MeV. This first isomer is separated from the ground state by an inner barrier, the top of which is located around Q_{20}=28 b, whose height amounts to 9.98 MeV. In our previous study [18], we have already explored the well kown reduction of the inner barrier due to triaxiality [15, 34] for a selected set of Uranium, Plutonium and superheavy nuclei for which experimental data are available [7, 43–46]. Such a lowering of the inner barriers comes with an increase of the collective inertia [32, 74] that tends to compensate the value of the action. As a result, the influence of triaxiality on the predicted spontaneous fission half-lives is quite limited [32, 33] and has not been considered in the present study. From Fig. 3 (a), one also observes the second and third fission barriers as well as a second fission isomer in between them at Q_{20}=94 b. This second isomer lies 4.29 MeV above the ground state. As we will see later on, second fission isomers are also obtained for other Plutonium nuclei [18].

The proton (dashed lines) and neutron (full lines) pairing interaction energies [21] are shown in Fig. 3 (b). The neutron energies exhibit minima at the spherical configuration, around the top of the inner and second fission barriers as well as around Q_{20}=110 b. On the other hand, the values of the octupole and hexadecupole moments

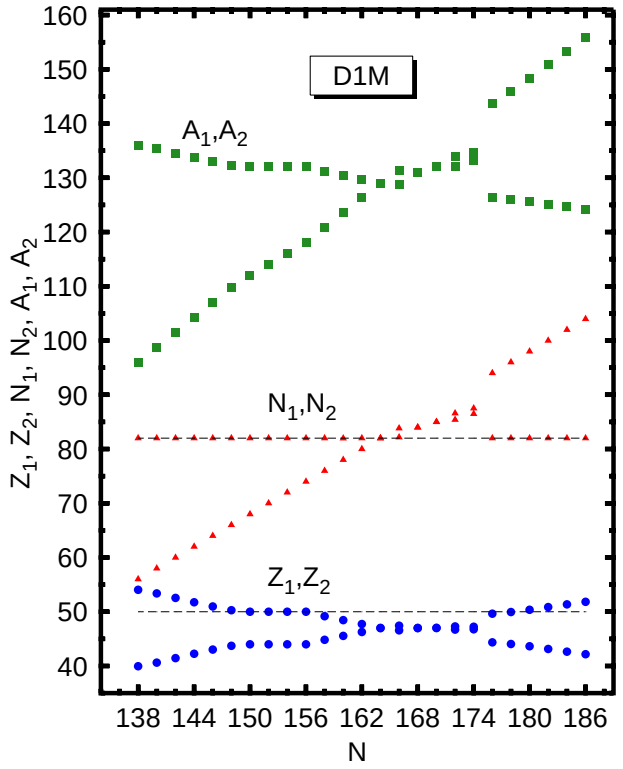

FIG. 8: (Color online) The proton (Z_1, Z_2), neutron (N_1, N_2) and mass (A_1, A_2) numbers of the two fragments resulting from the fission of the isotopes $^{232-280}$Pu are shown as functions of the neutron number in the parent nucleus. Results have been obtained with the Gogny-D1M EDF. The magic proton Z=50 and neutron N=82 numbers are highlighted with dashed horizontal lines to guide the eye.

corresponding, to the 1F [i.e., $Q_{30}(1F)$ and $Q_{40}(1F)$] and 2F [i.e., $Q_{30}(2F)$ and $Q_{40}(2F)$] curves in Fig. 3 (c) clearly reflect the separation of those paths in the multidimensional space of parameters.

In Fig. 3 (d), we have plotted the collective masses obtained within the ATDHFB scheme. The GCM masses (not shown in the figure) display a similar trend but are, on the average, always smaller than the corresponding ATDHFB values. Such differences between the ATDHFB and GCM masses have also been found in previous studies [17, 18, 70] and can lead to differences of several orders of magnitud in the predicted t_{SF} values. This is the reason why both the ATDHFB and GCM collective masses have been used in the present work to compute spontaneous fission half-lives. One should also keep in mind, that the collective inertias are computed in the perturbative cranking scheme [18, 63–65]. For example, for E_0=1.5 MeV, the t_{SF} values predicted within the ATDHFB and GCM schemes are 4.544×10^{32} s and 2.581×10^{25} s, respectively. Let us also mention, that the wiggles in the masses have been softened using a three point filter [18]. Since we take the 1F and 2F curves as intersecting and do not include the effect of the γ degree of freedom, the t_{SF} values reported in this work should be taken as lower bounds to the real ones.

In Fig. 4, we have plotted the density profiles for the nucleus ^{246}Pu at the 1F configurations with Q_{20}=60 and 140 b [panels (a) and (b)]. On the other hand, the corresponding 2F solution at Q_{20}=140 b is shown in Fig. 4 (c). It consists of a spherical ^{132}Sn fragment and an oblate and slightly octupole deformed ^{114}Ru fragment with β_2=-0.23 and β_3=0.02 (referred to the fragment's center of mass). The oblate shape of the ^{114}Ru fragment minimizes a large Coulomb repulsion of 205.81 MeV.

Some comments are in order here. First, as we will see later on, oblate deformed fragments are also obtained in our calculations for other Plutonium isotopes. Similar results have already been obtained in previous studies of the Uranium isotopes [17, 18] and deserve further attention as only prolate deformations are usually assumed for fission fragments [5, 6]. Second, as discussed in previous works [75–77], the likelihood of obtaining the ^{132}Sn fragment is related to the key role played by the magic proton Z=50 and neutron N=82 numbers. This is not surprising as such a distribution is obtained applying the Ritz variational principle [78] to the corresponding HFB energy. However, the comparison with the experimental data [45, 46] reveals that the 2F configurations resulting from minimizing the HFB energy are not necessarily the ones arising after scission. For example, for nuclei in the considered region of the nuclear chart, the experimental mass number of the heavy fragment is close to A=140 instead of the value A=132 obtained in our calculations. In our (minimal energy) calculations the properties of the fragments are determined from 2F solutions at the largest quadrupole moments. If, on the other hand, we take the breaking point as the one where the neck reaches a critical value [79] the predicted heavy fragment mass number turns out to be closer to the experimental one [18]. Last, but not least, the predicted masses should be taken as an approximation to the peaks of the experimental broad mass distribution of the fragments. In order to account for prescission quantum shell effects as well as the broad mass distribution a more sophisticated (dynamical) approach than ours is needed (see, for example, [80, 81] and references therein). We will not pursue this kind of computationally involved approximation in the present study and simply keep in mind that the mass distribution of the fragments leading to the minimal HFB energy slightly underestimates the heavy fragment mass.

In Fig. 5 we have plotted the energies $E_{HFB} + \Delta E_{ROT}$ for the nuclei $^{232-256}$Pu [panel (a)] and $^{258-280}$Pu [panel (b)]. Both the 1F (full lines) and 2F (dashed lines) curves are shown in the plots. Starting from ^{234}Pu (^{260}Pu) in panel (a) [in panel (b)] all the curves have been successively shifted by 20 MeV in order to accomodate them in a single plot. The first apparent feature from the figure, is the gradual decreasing of the ground state deformations as we move towards the neutron dripline reaching Q_{20}=2-6 b in the heavier isotopes. Note, that the deformed ground states in $^{272-280}$Pu are a direct consequence of the approximate restoration of the broken

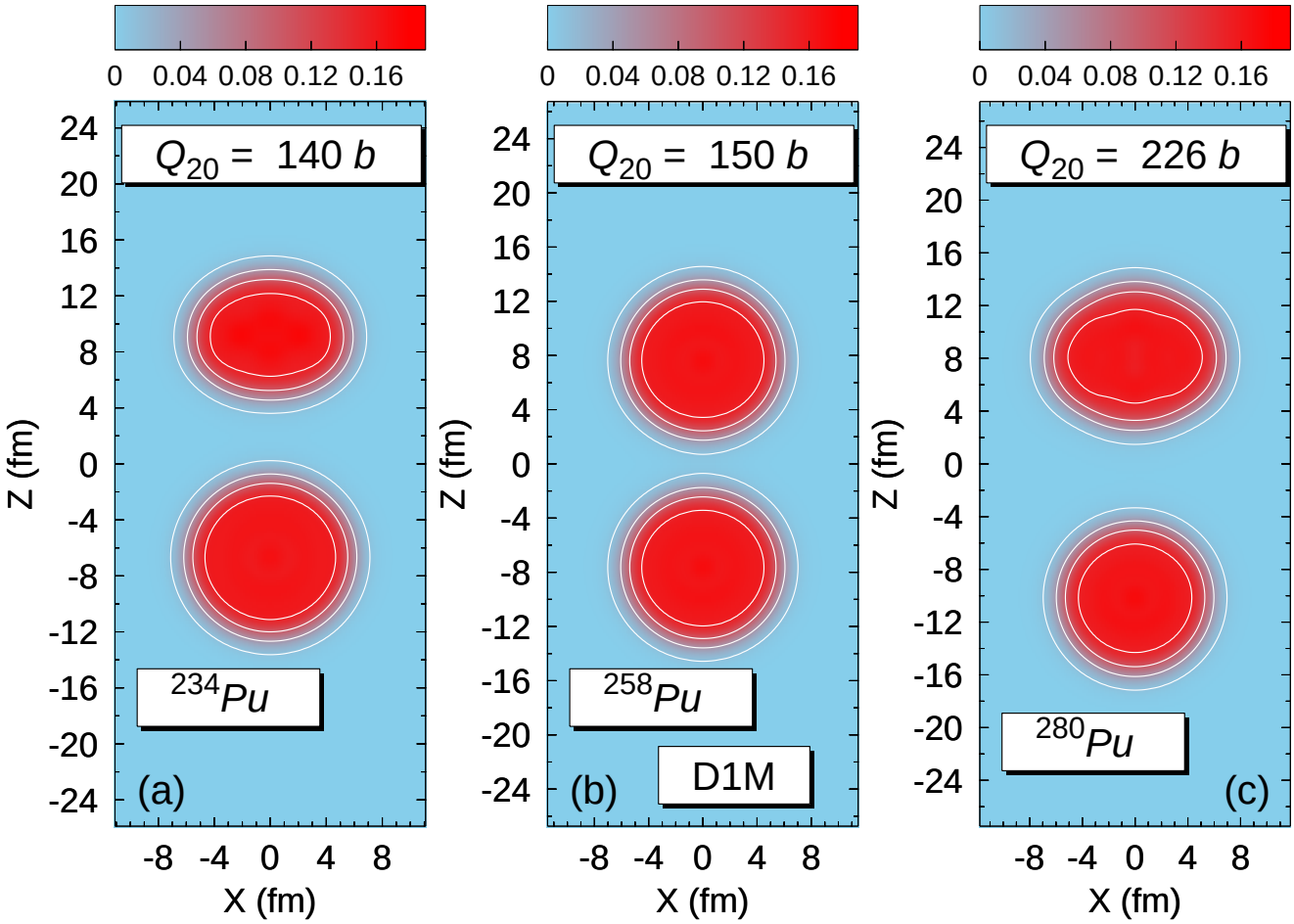

FIG. 9: (Color online) Density contour plots for the nuclei ^{234}Pu [panel (a)], ^{258}Pu [panel (b)] an ^{280}Pu [panel (c)]. The density profiles correspond to 2F solutions at the quadrupole deformations Q_{20}=140, 150 and 226 b, respectively. Results are shown for the Gogny-D1M EDF. Densities are in units of fm^{-3} and contour lines are drawn at 0.01, 0.05, 0.10 and 0.15 fm^{-3}.

rotational symmetry [18, 66, 68, 82] . However, from the (intrinsic) HFB point of view the nuclei $^{272-280}$Pu are spherical. The neutron pairing energy only vanishes at Q_{20}=0 for ^{278}Pu. In addition, we have computed the two-neutron separation energies that reveal a sudden drop at N=186. Both are clear signatures of the magicity of the neutron number N=184. On the other hand, the inner barrier heights increase and the 1F curves widen for increasing neutron number. The previous results agree well with the ones obtained for Uranium isotopes [17, 18] as well as with the Extended Thomas-Fermi calculations of Ref. [83] which predicted very high barrier heights for N=184 isotones in this region of the nuclear chart.

Another prominent feature from Fig.5 is the appearence of second fission isomers in the 1F curves of several of the considered Plutonium isotopes. Such second isomers have been predicted within the microscopic-macroscopic (MM) approach [8–10, 13, 14] as well as in several self-consistent calculations [11, 12, 15]. They have also been found in our previous HFB study [18] for the nuclei $^{232-280}$U regardless of the particular version of the Gogny-EDF employed. Moreover, the results discussed in the present work and the ones in Refs. [16–18], based on different EDFs, show that the shell effects leading to fission isomers in the corresponding 1F curves of Uranium, Plutonium and Thorium nuclei are systematically present in different mean-field calculations. The issue of why mean-field calculations do not reproduce the scarce experimental data deserves further consideration.

In Fig. 6, we have plotted the excitation energies E_I (E_{II}) and the barrier heights B_I (B_{II}) for the first (second) isomeric wells in panel (a) [panel (b)], as functions of the neutron number N, for the nuclei $^{232-280}$Pu. From Fig. 6 (a), we observe that the barrier heights B_I exhibit a sudden drop at N=168 while the excitation energies E_I of the first fission isomers remain relatively constant up to the same neutron number. For larger neutron numbers E_I increases linearly up to N=184 where both E_I and B_I display a sudden drop which is characteristic of the filling of a new major shell. The barrier heights B_{II}, shown in Fig. 6 (b), display two maxima, one at N=150 and the other at N=178. On the other hand, similar to E_I, the excitation energies E_{II} increase linearly for N $\geq$ 168 and display a sudden drop at N=184. Another

relevant feature from Fig. 6 (b) is the lack of a second isomeric well for some light isotopes. For a comparison of the excitation energies of fission isomers in $^{238-242}$Pu, the reader is referred to Ref. [18].

In our previous work [18], we have also explored the role of the γ degree of freedom for configurations around the top of the inner barrier in a selected set of nuclei for which experimental data are available [7, 43–46] . In the case of $^{238-244}$Pu, for example, triaxiality reduces the predicted B_I values by 1.11, 1.75, 2.23 and 2.74 MeV, respectively, though the theoretical values are still larger than the experimental ones. The same overestimation is also observed for the outer barriers, though the inclusion of reflection asymmetric shapes leads to a reduction of a few MeV. Ours and previous calculations for nuclei in this region [15, 18], seem to suggest that other effects not explicitly taken into account in this work may be required to improve the agreement with the available experimental data. Among them, the pairing degrees of freedom and/or the collective dynamics appear as plausible candidates to be considered in future work. However, one should keep in mind that the experimental data for barrier heights are model dependent and therefore less reliable than the corresponding fission half-lives for a comparison with theoretical values.

Let us now turn our attention to the spontaneous fission half-lives predicted for the isotopes $^{232-280}$Pu within the GCM and ATDHFB schemes. They are depicted in Fig.7 as functions of the neutron number. Calculations have been carried out with E_0=0.5, 1.0, 1.5 and 2.0 MeV, respectively. The experimental t_{SF} values [44] for $^{236-244}$Pu are also included in the plot. The ATDHFB t_{SF} values are always larger than the GCM ones. For example, for ^{234}Pu (E_0=1.5 MeV) the GCM and ATDHFB values are 1.841×10^{18} s and 4.864×10^{25} s while for ^{250}Pu the corresponding values are 7.384×10^{21} s and 3.146×10^{28} s, respectively. The differences between the GCM and ATDHFB fission half-lives increase with increasing neutron number reaching 22 orders of magnitud for ^{278}Pu. On the other hand, increasing E_0 always leads to smaller t_{SF} values. For the isotopes with neutron number $N \geq 166$ we observe a steady increase in the spontaneous fission half-lives reaching a maximum for the magic neutron number N=184.

In Fig. 7, we have also plotted the α-decay half-lives t_α computed with the parametrization given in Ref. [71]. We have used the binding energies obtained for the corresponding Plutonium and Uranium nuclei. Let us stress that the parametrization D1M is well suited for such calculations since it has been tailored to provide a better description of the nuclear masses [49] than the standard Gogny-D1S [23] EDF. As can be seen, for increasing neutron number fission turns out to be faster than α-decay. For Plutonium isotopes, our calculations predict the crossing point to be $N \approx 160$, i.e., around two mass units later than the D1M value found for Uranium isotopes [18].

In Fig.8 we have plotted the proton (Z_1, Z_2), neutron

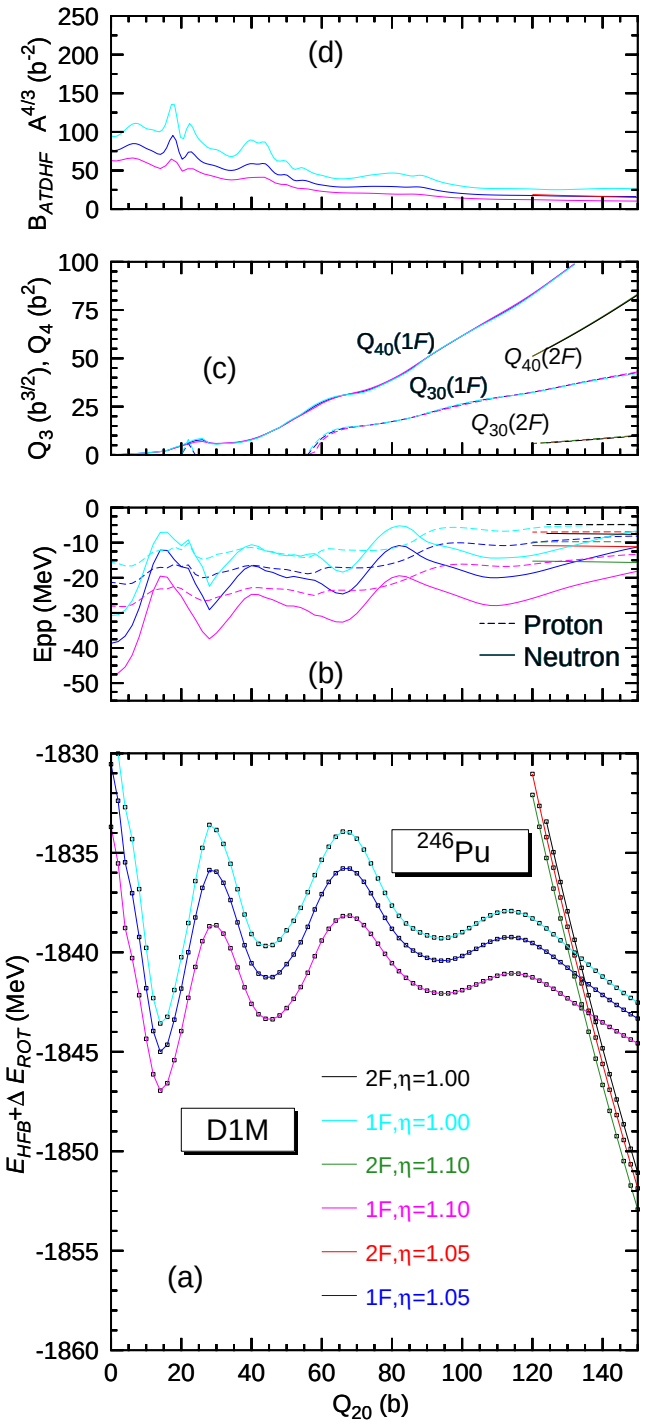

FIG. 10: (Color online) The HFB plus the zero point rotational energies obtained with the normal (η=1.00) and modified (η=1.05 and 1.10) Gogny-D1M EDFs are plotted in panel (a) as functions of the quadrupole moment Q_{20} for the nucleus ^{246}Pu. For each η value, both the one (1F) and two-fragment (2F) solutions are included in the plot. The pairing interaction energies are depicted in panel (b) for protons (dashed lines) and neutrons (full lines). The octupole and hexadecapole moments corresponding to the 1F and 2F solutions are given in panel (c). The collective masses obtained within the ATDHFB approximation are plotted in panel (d). For more details, see the main text.

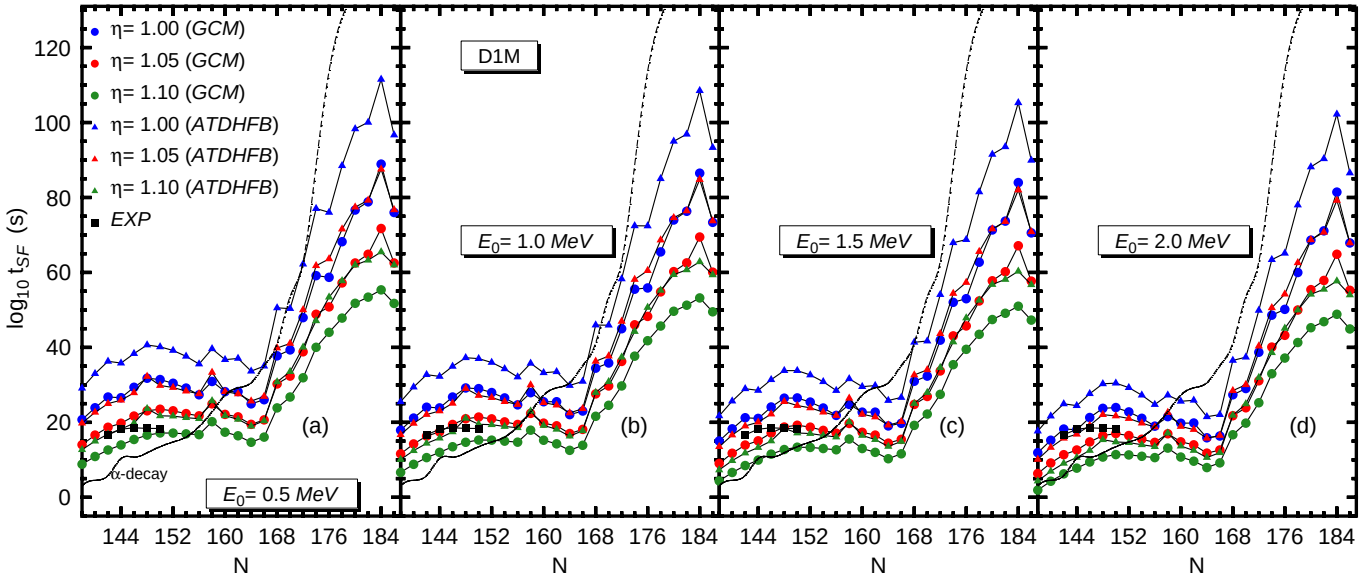

FIG. 11: (Color online) The spontaneous fission half-lives t_{SF}, predicted within the GCM and ATDHFB schemes, for the isotopes $^{232-280}$Pu are depicted as functions of the neutron number. Results have been obtained with the normal (η=1.00) and modified (η=1.05 and 1.10) Gogny-D1M EDFs. Calculations have been carried out with E_0=0.5 [panel (a)], 1.0 [panel (b)], 1.5 [panel (c)] and 2.0 MeV [panel (d)], respectively. The experimental t_{SF} values [44] for $^{236-244}$Pu are included in the plot. In addition, α-decay half-lives are plotted with short dashed lines. For more details, see the main text.

(N_1, N_2) and mass (A_1, A_2) numbers corresponding to the 2F configurations in $^{232-280}$Pu. In all cases, the 2F solutions have been taken for the largest quadrupole deformations available so as to guarantee that fragment properties are nearly independent of the quadrupole moment. Once more, one clearly sees the key role played by both the neutron N=82 and proton Z=50 magic numbers in the masses and charges of the predicted fission fragments. However, as already explained above in the case of ^{246}Pu, in our calculations the properties of the fragments have been determined using minimal energy criteria. Therefore, caution should be taken when comparing with the experiment [45, 46, 84].

Finally, in Fig. 9 we have plotted the density contours for the nuclei ^{234}Pu [panel (a)], ^{258}Pu [panel (b)] and ^{280}Pu [panel (c)]. The 2F solutions correspond to the quadrupole deformations Q_{20}=140, 150 and 226 b, respectively. The lighter and heavier fragments in ^{234}Pu and ^{280}Pu are predicted to be oblate (β_2=-0.21) and slightly octupole (β_3=0.01) deformed. Oblate deformed fragments have also been obtained for other Plutonium and Uranium nuclei [17, 18]. They deserve further study as only prolate deformations are usually assumed [5, 6] for fission fragments. On the other hand, for ^{258}Pu our Gogny-D1M calculations predict a symmetric splitting into two spherical fragments.

C. Varying pairing strengths in Plutonium isotopes

In this section we explicitly consider the impact of pairing correlations on the predicted t_{SF} values for $^{232-280}$Pu. To this end, both the proton and neutron pairing fields [21] of the Gogny-D1M EDF (η=1) has been scaled by the same factors η=1.05 and 1.10, respectively [17, 18].

Let us briefly summarize our findings in the case of ^{246}Pu, taken as an illustrative outcome of our calculations. The rotationally corrected 1F and 2F HFB energies obtained with the normal (η=1.00) and modified (η=1.05 and 1.10) Gogny-D1M EDFs are plotted in Fig. 10 (a), as functions of the quadrupole moment Q_{20}. Regardless of the η value, the 1F and 2F curves display similar profiles in all the considered isotopes and are shifted downward with increasing η values. As expected, the proton (dashed lines) and neutrons (full lines), pairing interaction energies shown in Fig. 10 (b), become larger with increasing η values. On the other hand, the multipole moments shown in Fig. 10 (c) are nearly independent of η and lie on top of each other.

As a consequence of the inverse dependence of the collective masses with the square of the pairing gap [57, 58], the ATDHFB collective masses, depicted in Fig. 10 (d), are strongly correlated with the corresponding η values. The same is also true for the GCM masses (not shown in the plot). For example, the ATDHFB and GCM masses are reduced by 30 % and 24 % for η=1.05 while for η=1.10 they are reduced by 50 % and 40 %, respectively. These reductions change the predicted spontaneous fission half-lives by several orders of magnitud. For example, for E_0=1.0 MeV, we have obtained within the ATDHFB scheme t_{SF}= 9.504 $\times$ 10^{35}, 4.171 $\times$ 10^{26} and 2.417 $\times$ 10^{19} s for η=1.00, 1.05 and 1.10, respectively. The corresponding GCM values turn out to be 8.999 $\times$ 10^{27}, 8.440

$\times 10^{20}$ and 1.831×10^{15} s.

The spontaneous fission half-lives t_{SF}, predicted within the GCM and ATDHFB schemes, for the isotopes $^{232-280}$Pu are depicted, as functions of the neutron number, in Fig. 11. Results have been obtained with the normal (η=1.00) and modified (η=1.05 and 1.10) Gogny-D1M EDFs. Calculations have been carried out with E_0=0.5 [panel (a)], 1.0 [panel (b)], 1.5 [panel (c)] and 2.0 MeV [panel (d)], respectively. The experimental t_{SF} values [44] for $^{236-244}$Pu are included in the plot. In addition, α-decay half-lives [71] are plotted with short dashed lines. The results shown in Fig. 11 clearly demonstrate, regardless of the ATDHFB and/or GCM scheme used, the strong impact of pairing correlations on the predicted t_{SF} values. Note that, for example, our theoretical values for $^{236-244}$Pu agree reasonably well with the experimental ones. It is quite satisfying to see that, in spite of the large variability in the predicted t_{SF} values, the main findings previously summarized in Fig. 7 still hold. On the one hand, these results and the ones discussed in Sec. III B corroborate the predictive power of the Gogny-D1M EDF when used to describe fission along isotopic chains [18]. On the other hand, they also point to the use of experimental fission data to fine tune the pairing strengths in those EDFs commonly employed in fission calculations.

IV. CONCLUSIONS

In this paper we have considered, for the first time, the systematic microscopic description of fission along the Plutonium chain, including very neutron-rich isotopes, based on the Gogny-D1M EDF. In addition, we have further validated the use of the parametrization D1M to describe the fission properties of heavy nuclear systems through the computation of the spontaneous fission half-lives in $^{242-262}$Fm and their comparison with the available experimental data.

We have resorted to the methodology already employed in Ref.[18] to determine the fission paths (i.e., the 1F and 2F HFB solutions) in $^{232-280}$Pu and $^{242-262}$Fm. In particular, we have considered constraints on the proton $\hat{Z}$ and neutron $\hat{N}$ numbers as well as on the (axially symmetric) quadrupole $\hat{Q}_{20}$, octupole $\hat{Q}_{30}$, necking $\hat{Q}_{Neck}(z_0, C_0)$ and $\hat{Q}_{10}$ operators. Zero point rotational and vibrational quantum corrections have always been added to the corresponding 1F and 2F HFB configurations in an approximate projection-after-variation (PAV) framework [21].

The spontaneous fission half-lives t_{SF} for the considered nuclei, have been computed within the standard WKB approximation combined with microscopically determined state-of-the-art input resulting from the Gogny-D1M HFB calculations. The uncertainties arising from such an input have been critically addressed. We have paid especial attention to the impact of pairing correlations on the spontaneous fission half-lives in $^{232-282}$Pu. Similar to the results obtained for the nuclei $^{232-282}$U [18], we have found that changes of 5 % and 10 % in the pairing strengths of the original Gogny-D1M EDF already lead to differences of several orders of magnitud in the theoretical t_{SF} values. Let us stress that HFB calculations, based on the D1S and D1N Gogny-EDFs, have also been performed for the isotopes $^{232-282}$Pu. They reveal similar trends and variability as the ones discussed in this study. From these results we conclude that, regarless of the particular parametrization of the Gogny-EDF employed, pairing correlations have a strong impact on the absolute values of fission observables in Uranium, Plutonium and other heavy nuclei. This is further corroborated from the recent results obtained with the Barcelona-Catania-Paris-Madrid (BCPM) EDF [17]. Therefore, our calculations point to the use of fission data to fine tune the pairing strengths of those EDFs commonly employed in microscopic nuclear structure studies.

Nevertheless, in spite of the large variability observed in the results, a clear pattern emerges as a function of the mass number in Uranium and Plutonium nuclei: the t_{SF} values remain relatively constant up to N=166-168 and from there on they increase almost linearly up to a maximum at the magic neutron number N=184. For increasing neutron number fission becomes faster than α-decay. For Plutonium isotopes, our calculations predict the crossing point to be around two mass units later (i.e., N $\approx$ 160) than for Uranium isotopes. In addition, the 1F curves obtained for several Plutonium isotopes reveal that the shell effects responsible for the appearence of second fission isomers in this region of the nuclear chart are systematically present in ours and other mean-field calculations [16–18]. A detailed investigation of those shells effects as well as the relation between second isomeric and dimolecular states in the framework of our calculations is in progress and will be reported elsewhere.

In our calculations the masses and charges of the fission fragments are determined from 2F solutions obtained applying the Ritz variational principle to the HFB energy. Such an approximation, overestimates the role of the proton Z=50 and neutron N=82 magic numbers to determine the properties of the fission fragments. In particular, we have found a systematic overestimation of the heavy fragment's mass resulting from fissioning both Uranium and Plutonium nuclei. This indicates the need of a more sophisticated approximation than ours able to account for prescission quantum shell effects as well as the broad mass distribution of the fission fragments [80, 81].

Though in this and in our previous study [18] we have shown that the Gogny-D1M HFB framework does provide a reasonable starting point, it is also clear that some of its defficiencies are deeply rooted in the description of fission resorting to minimal energy criteria. Here, alternatives approaches based on a minimal action, instead of a minimal energy, path [85] deserve further consideration. Having in mind the strong impact of pairing correlations on the predicted spontaneous fission half-lives

such theories should incorporate, in addition to the multipole moments, the minimization of the action Eq.(3) with respect to pairing fluctuations arising from the broken U(1) number symmetry in the intrinsic HFB states used to label the different fission configurations. Work along these lines is in progress and will be reported in a shortcoming publication.

Acknowledgments

Work supported in part by MICINN grants Nos. FPA2012-34694, FIS2012-34479 and by the Consolider-Ingenio 2010 program MULTIDARK CSD2009-00064. One of us (R.R), would like to thank the warm hospitality received at the Department of Physics, Kuwait University, during the first stages of this work.

[1] H.J. Specht, Rev. Mod. Phys. **46**, 773 (1974).
[2] S. Björnholm and J.E. Lynn, Rev. Mod. Phys. **52**, 725 (1980).
[3] C. Wagemans, *The Nuclear Fission Process* (CRC Press, Boca Raton, 1991).
[4] H.J. Krappe and K. Pomorski, *Theory of Nuclear Fission*, Lectures Notes in Physics, **838** (2012).
[5] P. Möller and A. Iwamoto, Phys. Rev. C **61**, 047602 (2000).
[6] P. Möller, D.G. Madlan, A.J. Sierk and A. Iwamoto, Nature **409**, 785 (2001).
[7] B. Singh, R. Zywina and R. Firestone, Nucl. Data Sheets **97**, 241 (2002).
[8] V. V. Pashkevich, Nucl. Phys. A **169**, 275 (1971).
[9] P. Möller, Nucl. Phys. A **192**, 529 (1972).
[10] M. Kowal and J. Skalski, Phys. Rev. C **85**, 061302 (2012).
[11] J. F. Berger, M. Girod and D. Gogny, Nucl. Phys. A **502**, 85 (1989).
[12] K. Rutz, J. Marhun, P. -G. Reinhard and W. Greiner, Nucl. Phys. A **590**, 680 (1995).
[13] S. Ćwiok, W. Nazarewicz, J. Saladin, W. Plóciennik and A. Johnson, Phys. Lett. B **322**, 304 (1994).
[14] R. Bengtsson, I. Ragnarsson, S. Aberg, A. Gyurkovich, A. Sobiczewski and K. Pomorski, Nucl. Phys. A **473**, 77 (1987).
[15] J.-P. Delaroche, M. Girod, H. Goutte and J. Libert, Nucl. Phys. A **771**, 103 (2006).
[16] J.D. McDonnell, W. Nazarewicz and J.A. Sheikh, Phys. Rev. C **87**, 054327 (2013).
[17] S.A. Giuliani and L.M Robledo, Phys. Rev. C **88**, 054325 (2013).
[18] R. Rodríguez-Guzmán and L.M. Robledo, Phys. Rev. C **89**, 054310 (2014).
[19] J. W. Negele, Nucl. Phys. A **502**, 371 (1989).
[20] J. Skalski, Phys. Rev. C **77**, 064610 (2008).
[21] P. Ring and P. Schuck, *The Nuclear Many-Body Problem* (Springer, Berlin, 1980).
[22] M. Bender, P.-H. Heenen and P.-G. Reinhard, Rev. Mod. Phys. **75**, 121 (2003).
[23] J. F. Berger, M. Girod, and D. Gogny, Nucl. Phys. A **428**, 23c (1984).
[24] V. Martin and L.M. Robledo, Int. J. Mod. Phys. E **18**, 788 (2009).
[25] N. Dubray, H. Goutte and J.-P. Delaroche, Phys. Rev. C **77**, 014310 (2008).
[26] S. Pérez-Martín and L.M. Robledo, Int. J. Mod. Phys. E **18**, 861 (2009).
[27] W. Younes and D. Gogny, Phys. Rev. C **80**, 054313 (2009).
[28] M. Warda, J. L. Egido, L.M. Robledo and K. Pomorski, Phys. Rev. C **66**, 014310 (2002).
[29] M. Warda and J.L. Egido, Phys. Rev. C **86**, 014322 (2012).
[30] N. Nikolov, N. Schunck, W. Nazarewicz, M. Bender and J. Pei, Phys. Rev. C **83**, 034305 (2011).
[31] J. Erler, K. Langanke, H.P. Loens, G. Martínez-Pinedo and P.-G. Reinhard, Phys. Rev. C **85**, 025802 (2012).
[32] A. Baran, K. Pomorski, A. Lukasiak and A. Sobiczewski, Nucl. Phys. A **361**, 83 (1981).
[33] S. Ćwiok, P. -H. Heenen and W. Nazarewicz, Nature **433**, 705 (2005).
[34] H. Abusara, A.V. Afanasjev and P. Ring, Phys. Rev. C **82**, 044303 (2010).
[35] H. Abusara, A.V. Afanasjev and P. Ring, Phys. Rev. C **85**, 024314 (2012).
[36] B.-N. Lu, E.-G. Zhao and S.-G. Zhou, Phys. Rev. C **85**, 011301 (2012).
[37] S. Karatzikos, A. V. Afanasjev, G. A. Lalazissis and P. Ring, Phys. Lett. B **689**, 72 (2010).
[38] A. Sobiczewski and K. Pomorski, Prog. Part. Nucl. Phys. **58**, 292 (2007).
[39] R. Julin, Nucl. Phys. A **834**, 15c (2010)
[40] Yu.Ts. Oganessian, F.Sh. Abdullin, S.N. Dmitriev, J.M. Gostic, J.H. Hamilton, R.A. Henderson, M. G. Itkis, K.J. Moody, A.N. Polyakov, A.V. Ramayya, J.B. Roberto, K.P. Rykaczewski, R.N. Sagaidak, D.A. Shaughnessy, I.V. Shirokovsky, M.A. Stoyer, V.G. Subbotin, A.M. Sukhov, Yu.S. Tsyganov, V.K. Utyonkov, A.A. Voinov and G.K. Vostokin, Phys. Rev. Lett. **108**, 022502 (2012).
[41] H. Haba, D. Kaji, H. Kikunaga, Y. Kudou, K. Morimoto, K. Morita, K. Ozeki, T. Sumita, A. Yoneda, Y. Kasamatsu, Y. Komori, K. Ooe and A. Shinohara, Phys. Rev. C **83** (2011) 034602.
[42] M. Arnould, S. Goriely and K. Takahashi, Phys. Rep. **450**, 97 (2007).
[43] R. Capote et al., Nucl. Data Sheets **110**, 3107 (2009).
[44] N.E. Holden and D.C. Hoffman, Pure Appl. Chem. **72**, 1525 (2000).
[45] L. Dematté, C. Wagemans, R. Barthélémy, R. Dh́ont and A. Deruytter, Nucl. Phys. A **617**, 331 (1997).

[46] D.C. Hoffman and M.M. Hoffman, Ann. Rev. Nucl. Sci. **24**, 151 (1974).

[47] J. Dechargé and D. Gogny, Phys. Rev. C **21**, 1568 (1980).

[48] F. Chappert, M. Girod, and S. Hilaire, Phys. Lett. B **668**, 420 (2008).

[49] S. Goriely, S. Hilaire, M. Girod and S. Péru, Phys. Rev. Lett. **102**, 242501 (2009).

[50] R. Rodríguez-Guzmán, L.M. Robledo and P. Sarriguren, Phys. Rev. C **86**, 034336 (2012).

[51] L.M. Robledo and R. Rodríguez-Guzmán, J. Phys. G: Nucl. Part. Phys. **39**, 105103 (2012).

[52] R. Rodríguez-Guzmán, L.M. Robledo, P. Sarriguren and J. E. García-Ramos, Phys. Rev. C **81**, 024310 (2010).

[53] R. Rodríguez-Guzmán, P. Sarriguren, L.M. Robledo, and S. Perez-Martin, Phys. Lett. B **691**, 202 (2010).

[54] L.M. Robledo, R. Rodríguez-Guzmán, and P. Sarriguren, J. Phys. G: Nucl. Part. Phys. **36**, 115104 (2009).

[55] R. Rodríguez-Guzmán, P. Sarriguren, and L.M. Robledo, Phys. Rev. C **82**, 061302(R) (2010).

[56] R. Rodríguez-Guzmán, P. Sarriguren, and L.M. Robledo, Phys. Rev. C **83**, 044307 (2011).

[57] M. Brack, J. Damgaard, A.S. Jensen, H.C. Pauli, V.M Strutinsky and C.Y. Wong, Rev. Mod. Phys. **44**, 320 (1972).

[58] J.F. Berstch and H. Flocard, Phys. Rev. C **43**, 2200 (1991).

[59] L.M. Robledo and G. F. Berstch, Phys. Rev. C **84**, 014312 (2011).

[60] C. Titin-Schnaider and Ph. Quentin, Phys. Lett. B **49**, 213 (1974).

[61] M. Anguiano, J. L. Egido and L. M. Robledo, Nucl. Phys. A **683**, 227 (2001).

[62] N. Dubray and D. Regnier, ArXiv/nucl-th/1112.4196 (2012).

[63] M. Girod and B. Grammaticos, Nucl. Phys. A **330**, 40 (1979).

[64] M.J. Giannoni and P. Quentin, Phys. Rev. C **21**, 2060 (1980); Phys. Rev. C **21**, 2076 (1980).

[65] J. Libert, M. Girod and J.P. Delaroche, Phys. Rev. C **60**, 054301 (1999).

[66] R. Rodríguez-Guzmán, J.L. Egido and L.M. Robledo, Phys. Lett. B **474**, 15 (2000); Phys. Rev. C **62**, 054308 (2000).

[67] J.L. Egido and L.M.Robledo, Lectures Notes in Physics **641**, 269 (2004).

[68] R. Rodríguez-Guzmán, J.L. Egido, and L.M. Robledo, Nucl. Phys. A **709**, 201 (2002).

[69] A. Baran, Phys. Lett. B **76**, 8 (1978).

[70] A. Baran, J. A. Sheikh, J. Dobaczewski, W. Nazarewicz and A. Staszczak, Phys. Rev. C **84**, 054321 (2011).

[71] T. Dong and Z. Ren, Eur. Phys. J. A **26**, 69 (2005).

[72] S. Hilaire and M. Girod, Eur. Phys. J. A **33**, 237 (2007).

[73] A. Staszczak, A. Baran, J. Dobaczewski and W. Nazarewicz, Phys. Rev. C **80**, 014309 (2009).

[74] M. Bender, K. Rutz, P.-G. Reinhard, J.A. Maruhn and W. Greiner, Phys. Rev. C **58**, 2126 (1998).

[75] N. Nenoff, P. Bringel, A. Bürger, S Chmel, S. Dababneh, M. Heil, H. Hübel, F. Käppeler, A. Neusser-Neffgen and R. Plag, Eur. Phys. J. A **32**, 165 (2007).

[76] M. Piessens, E. Jacobs, S. Pommé and D. D. Frenne, Nucl. Phys. A **556**, 88 (1993).

[77] G. M. Ter-Akopian, J. H. Hamilton, Yu. Ts. Oganessian, A. V. Daniel, J. Kormicki, A. V. Ramayya, G. S. Popeko, B. R. S. Babu, Q.-H. Lu, K. Butler-Moore, W. -C. Ma, S. Ćwiok, W. Nazarewicz, J. K. Deng, D. Shi, J. Kliman, M. Morhac, J. D. Cole, R. Aryaeinejad, N. R. Johnson, I. Y. Lee, F. K. McGowan and J. X. Saladin, Phys. Rev. Lett. **77**, 32 (1996).

[78] J.-P. Blaizot and G. Ripka, *Quantum Theory of Finite Fermi Systems* (The MIT Press, Cambridge, MA, 1985).

[79] B. D. Wilkins, E. P. Steinberg and R. R. Chasman, Phys. Rev. C **14**, 1832 (1976).

[80] H. Goutte, J. F. Berger, P. Casoli and D. Gogny, Phys. Rev. C **71**, 024316 (2005).

[81] S. Goriely, J. -L. Sida, J. -F. Lemaitre, S. Panebianco, N. Dubray, S. Hilare, A. Bauswein and H. -T. Janka, ArXiv/astro-ph.SR/1311.5897 (2013).

[82] R. Rodríguez-Guzmán, J.L. Egido and L.M. Robledo, Phys. Rev. C **69**, 054319 (2004).

[83] A. Mamdouth, J. M. Pearson, M. Rayet and F. Tondeur, Nucl. Phys. A **679**, 337 (2001).

[84] K.-H. Schmidt et al., Nucl. Phys. A **665**, 221 (2000).

[85] J. Sadhukhan, K. Mazurek, A. Baran, J. Dobaczewski, W. Nazarewicz and J. A. Sheikh, Phys. Rev. C **88**, 064314 (2013).